



**HAL**  
open science

# Carcinogenic dioxane detection using pristine and metal-doped 2D VSe<sub>2</sub>: Insights from density functional theory simulations

Sreejith Pallikkara Chandrasekharan, Seetha Lakshmy, Saju Joseph,  
Nandakumar Kalarikkal

## ► To cite this version:

Sreejith Pallikkara Chandrasekharan, Seetha Lakshmy, Saju Joseph, Nandakumar Kalarikkal. Carcinogenic dioxane detection using pristine and metal-doped 2D VSe<sub>2</sub>: Insights from density functional theory simulations. *Aip Advances*, 2023, 13 (6), pp.065024. 10.1063/5.0139779 . hal-04198629

**HAL Id: hal-04198629**

**<https://hal.science/hal-04198629>**

Submitted on 24 May 2024

**HAL** is a multi-disciplinary open access archive for the deposit and dissemination of scientific research documents, whether they are published or not. The documents may come from teaching and research institutions in France or abroad, or from public or private research centers.







L'archive ouverte pluridisciplinaire **HAL**, est destinée au dépôt et à la diffusion de documents scientifiques de niveau recherche, publiés ou non, émanant des établissements d'enseignement et de recherche français ou étrangers, des laboratoires publics ou privés.



Distributed under a Creative Commons Attribution 4.0 International License

RESEARCH ARTICLE | JUNE 16 2023

# Carcinogenic dioxane detection using pristine and metal-doped 2D VSe<sub>2</sub>: Insights from density functional theory simulations

Special Collection: [2022 Chemical Physics](#)Sreejith Pallikkara Chandrasekharan ; Seetha Lakshmy ; Saju Joseph  ; Nandakumar Kalarikkal  

AIP Advances 13, 065024 (2023)

<https://doi.org/10.1063/5.0139779>View  
OnlineExport  
Citation

## APL Energy

### Latest Articles Online!

[Read Now](#)

# Carcinogenic dioxane detection using pristine and metal-doped 2D VSe<sub>2</sub>: Insights from density functional theory simulations

Cite as: AIP Advances 13, 065024 (2023); doi: 10.1063/5.0139779

Submitted: 24 December 2022 • Accepted: 1 June 2023 •

Published Online: 16 June 2023



View Online



Export Citation



CrossMark

Sreejith Pallikkara Chandrasekharan<sup>1,2</sup>  Seetha Lakshmy,<sup>1</sup>  Saju Joseph<sup>1,3a)</sup>   
and Nandakumar Kalarikkal<sup>1,3,4a)</sup> 

## AFFILIATIONS

<sup>1</sup> International and Inter University Centre for Nanoscience and Nanotechnology, Mahatma Gandhi University, Kottayam, Kerala 686 560, India

<sup>2</sup> Univ. Rennes, INSA Rennes, CNRS, Institut FOTON – UMR 6082, F-35000 Rennes, France

<sup>3</sup> School of Nanoscience and Nanotechnology, Mahatma Gandhi University, Kottayam, Kerala 686 560, India

<sup>4</sup> School of Pure and Applied Physics, Mahatma Gandhi University, Kottayam, Kerala 686 560, India

<sup>a)</sup> Authors to whom correspondence should be addressed: [nkkalarikkal@mgu.ac.in](mailto:nkkalarikkal@mgu.ac.in) and [psajuoseph@gmail.com](mailto:psajuoseph@gmail.com)

## ABSTRACT

Dioxane (diethylene oxide) is a synthetic organic compound classified as heterocyclic ether, a potentially carcinogenic water toxicant. Prolonged exposure can cause eye irritation, carcinogenic liver reactions, and other severe issues. Therefore, efficient dioxane detectors are needed to be designed and developed. Inspired by the recent developments of 2D materials in biosensing, in this work, the dioxane detection potentiality of pristine and metal-doped (Al, Au, and Ag) 2D VSe<sub>2</sub> have been systematically examined using Density Functional Theory (DFT) based simulations. Among all the metallic dopants considered, Al binds energetically on the VSe<sub>2</sub> surface with an energy of  $-2.158$  eV. The adsorption of dioxane was studied by considering the electronic properties, adsorption energy, orbital interactions, and charge transfer. Our DFT calculation suggests that dioxane adsorption in Al-doped VSe<sub>2</sub> is more promising than the pristine and other metal-doped VSe<sub>2</sub> systems, due to the reasonable adsorption energy of  $-0.80$  eV, charge transfer of  $-0.567e$ , and strong orbital interaction between Al  $3p$  and O  $2p$  orbitals. Additionally, the room temperature structural solidity of the sensor has also been verified using the *ab initio* molecular dynamics simulations. The reported theoretical results inspire the fabrication and engineering of efficient dioxane sensors using Al-doped VSe<sub>2</sub>.

© 2023 Author(s). All article content, except where otherwise noted, is licensed under a Creative Commons Attribution (CC BY) license (<http://creativecommons.org/licenses/by/4.0/>). <https://doi.org/10.1063/5.0139779>

## I. INTRODUCTION

Rapid industrialization and population growth resulted in the discharge of large quantities of organic pollutants, undeniably contributing to water resource pollution.<sup>1–3</sup> Diethylene oxide (widely known as dioxane or 1,4-dioxane), classified as ether, with the chemical formula C<sub>4</sub>H<sub>8</sub>O<sub>2</sub>, is a colorless liquid with a soft sweet smell like dimethyl ether. Dioxane is used on a large scale to produce paper, textiles, electronics, cosmetics, etc. They are often regarded as a powerful solvent and stabilizer for chlorinated solvents in laboratory applications. It is well known that dioxane is an environmental water toxicant with high water solubility, hydrophilicity, long-term

stability, and non-bio-degradability. Their excess presence can contaminate the ground, surface, and drinking water and are highly dangerous to living beings. Long term exposure can elicit severe eye irritation and carcinogenic reactions in the liver in various species. As per the studies, nearly one-fifth of the public drinking water sources in the United States (US) have measurable quantities of dioxane.<sup>4</sup> The International Agency for Research on Cancer (IARC) and the US Environmental Protection Agency (USEPA) have categorized dioxane as a potential human carcinogen.<sup>5</sup> Moreover, the Agency for Toxic Substances and Disease Registry (ATSDR) designated dioxane as a superfund precedence category due to the chemical harmful effects and proclivity to pollute drinking water.<sup>4</sup> Because

of these implications, it is urgent to develop sensors that selectively detect and remove the dioxane molecules from the environment.

In recent years, many sophisticated physicochemical and biological approaches have been used to successfully remove dioxane from affected environments. The unique chemical features of dioxane, such as its low Henry's law constant, high water solubility, and coexistence with the chlorinated solvents and other contaminants, make efficient removal difficult.<sup>6</sup> Complex water treatment procedures can be utilized to eradicate trace contaminants of dioxane.<sup>5</sup> Some of these include the photoinduced oxidation method (UV/H<sub>2</sub>O<sub>2</sub>) to substantially eliminate the structure of organic chemical; and, the Fenton's reagent (Fe and H<sub>2</sub>O<sub>2</sub>), advanced oxidation processes using systems, such as ozone (O<sub>3</sub>)/H<sub>2</sub>O<sub>2</sub>, and H<sub>2</sub>O<sub>2</sub> - TiO<sub>2</sub> combined vacuum UV. The sonolytic decomposition chemistry of dioxane in an aqueous solution has also been investigated,<sup>7</sup> where dioxane is dissolved into smaller short-chain organic by-products using ultrasound, which can subsequently be destroyed more successfully by other methods like biological processes. Although several other advanced dioxane removal technologies, such as solid-phase microextraction (SPME), distillation, gas chromatography (GC), thermal methods, air stripping and membrane filtration techniques, etc., are incompetent due to their high rate of cost and energy consumption.<sup>8–11</sup> Recent studies including electrochemical dioxane-detection by using nickel oxide doped on neodymium oxide nanocomposites (NiO@Nd<sub>2</sub>O<sub>3</sub> NCs) embedded on glassy carbon electrode<sup>12</sup> and reduced graphene oxide-curcumin nanocomposite synthesized by a simple solution approach<sup>13</sup> promotes the need of developing this water pollutant.

However, properties, such as binding energy, adsorption geometry, adsorption configuration, charge transfer, etc., for detecting biomolecules cannot be directly determined by the time-consuming real experiment methods. Computational techniques are the best way to perform quantum mechanical calculations to analyze materials' various properties and phenomena and model them.

In this study, we have adopted the widely applicable quantum mechanical theoretical simulation approach called Density Functional Theory (DFT)<sup>14</sup> to analyze the molecular interactions. In these first-principle based calculations, the energy is represented as functionals of density. Many theoretical investigations have recently been conducted to search for novel materials for sensing applications. Interestingly, some cutting-edge theoretical research on SiCNT was conducted utilizing DFT simulations to examine the adsorption and removal of dioxane.<sup>15</sup> Furthermore, the DFT-D3/revPBE calculation is verified using the MP2 theoretical method. The study showed that dioxane has significant adsorption toward this nanotube, but the higher recovery time limits the practical usage. However, most traditional sensing materials have several flaws due to their low sensitivity and selectivity. The interaction of biomolecules with 2D material is mainly via physisorption because of weak van der Waals forces. By modifying the functional qualities of 2D materials, such as defects engineering hybrid structure formation, the adsorption performances of these materials may be enhanced. Usually, metallic doping methods are adopted in the studies of 2D materials. Its unique and robust coupling of electromagnetic properties gives a charge transferring nature. They form covalent bonds with neighboring atoms via charge transfer, improving the conductivity of the pristine 2D material and hence the sensing properties.

Transition-metal dichalcogenides (TMDCs) are emerging 2D materials with a stoichiometric formula of MX<sub>2</sub>. M denotes a transition metal element, such as Sc, V, Mo, Ti, or W, while X stands for a chalcogen element, such as Te, Se, or S. Here, a single layer of M atoms is stacked between the bi-layer of X atoms in this tri-layered structure, creating the layered structure X-M-X. Long-range van der Waals (VdW) forces dominate between these layers, resulting in the weak interaction. It exhibits unique photoelectronic, thermal, chemical, and mechanical properties,<sup>16,17</sup> making it promising for gas or biosensing applications.<sup>18–20</sup> The uniqueness of TMDCs is due to the presence of the *d* orbitals of the heavy metals, which causes a robust spin-orbit interaction, leads to valley polarization. The TMDCs have out-of-plane and broken in-plane mirror symmetry. The polymorphic nature of TMDC structures is a fascinating feature. TMDCs can be mainly classified into two structural phases: 2H and 1T.<sup>21,22</sup> The 2H is semiconducting, and the coordination of metal atoms is trigonal prismatic, while the 1T structure is metallic with octahedral coordination. In view of the above, it is reasonable to conclude that TMDCs offer enormous untapped potential as a future choice for numerous biomolecule sensing applications with their wide range of characteristics.

2D vanadium dichalcogenides (VX<sub>2</sub>), such as VSe<sub>2</sub>, VTe<sub>2</sub>, and VS<sub>2</sub>, have recently attracted much interest<sup>23–26</sup> due to their exceptional optical, electrical, and chemical characteristics. Our research focused on the 1T VSe<sub>2</sub> monolayer, a paramagnetic material where the vanadium atoms are surrounded by a trigonally deformed cage of selenium atoms in an octahedral environment.<sup>27</sup> Zhang *et al.*<sup>28</sup> used a chemical vapor deposition (CVD) approach to establish a van der Waals epitaxial strategy for synthesizing stable 1T VSe<sub>2</sub> nanosheets on mica. Surprisingly, these 2D structures have exceptional metallic characteristics, including the electrical conductivity up to 10<sup>6</sup> S m<sup>-1</sup>, higher than the other conductive 2D materials. Synthesizing VSe<sub>2</sub> monolayer also have been reported by effective methods, such as liquid exfoliation,<sup>29</sup> from [(SnSe)<sub>1.15</sub>]<sub>m</sub>(VSe<sub>2</sub>)<sub>n</sub> ferecrystals via physical vapor deposition,<sup>30</sup> low-pressure chemical vapor deposition (LPCVD),<sup>31</sup> etc. In very recent work, the potential of 1T VSe<sub>2</sub> for nitrobenzene detection was explored.<sup>26</sup> The DFT study reveals that the transition metal doped VSe<sub>2</sub> is more sensitive to nitrobenzene molecules.

Although some significant observational facts exist for dioxane sensing studies, evidence of investigating TMDCs as a sensing material, particularly monolayered VSe<sub>2</sub>, as a potential dioxane sensing material is unknown to the authors' available knowledge. In this current work, the adsorption and electronic properties of VSe<sub>2</sub> as a biosensor for dioxane have been examined using first principle-based DFT calculations. To overcome the weak interaction of VSe<sub>2</sub> monolayer toward dioxane, VSe<sub>2</sub> has been modified by doping with various metals (Al, Ag, Au, W, and Ti). Total Density of States (TDOS) and Partial Density of States (PDOS) analyses have been done to study the orbital interactions of states near the Fermi level and the charge transfer analysis via Lowdin Charge Analysis (LCA). Finally, because of its high adsorption energy toward dioxane, we suggest the Al-doped VSe<sub>2</sub> structure is among the most potential dioxane sensing materials. Furthermore, the structural durability of VSe<sub>2</sub> + Al was examined using *ab initio* MD simulations at 300 K, which revealed that the combination is extremely stable.



## II. COMPUTATIONAL DETAILS

This study calculated all the structural, electronic, interfacial, and sensing properties of 2D  $\text{VSe}_2$  and metal doped structures using DFT with the Quantum Espresso package.<sup>32</sup> As an exchange-correlation energy functional approximation, Perdew–Burke–Ernzerhof (PBE) in the Generalized Gradient Approximation (GGA) function (PBE-GGA) were used.<sup>33</sup> As per the literature, GGA is appropriate for accurately predicting the electronic, magnetic, and optical properties of 2D TMDCs. To accommodate the long-range van der Waals interactions, Grimme DFT-D2 were also introduced in the calculations. For the current work, we have modeled a  $2 \times 2$  supercell of 2D 1T  $\text{VSe}_2$  monolayer containing 12 atoms. To eliminate the interactions between the periodic images, a  $20 \text{ \AA}$  vacuum spacing is introduced in the vertical direction of the  $\text{VSe}_2$  monolayer, i.e., in the z-direction. The plane-wave-cutoff energy was set to 35 Ry. The geometrical structures were relaxed until each atom's total computed energy and force were less than  $10^{-6}$  and  $10^{-4}$  eV, respectively. The Brillion zone integration was achieved by  $4 \times 4 \times 1$  Monkrostr–Pack. For the most promising

system, molecular dynamic simulations at 300 K were also done to remark on the sensor material's integrity at ambient temperatures.

## III. RESULTS AND DISCUSSION

### A. Electronic and structural properties of $\text{VSe}_2$ monolayer

In this study, we have considered the 1T phase of pristine  $\text{VSe}_2$ , in which a layer of metal Vanadium is placed between two selenium sheets. The optimized  $2 \times 2$  supercell structure of  $\text{VSe}_2$  is displayed in Fig. 1(a). The obtained lattice constants are  $a = b = 3.334 \text{ \AA}$ , correlating neatly with published primitive cell experimental value,  $a = b = 3.356 \text{ \AA}$ <sup>34</sup> and  $a = b = 3.36 \text{ \AA}$ ,<sup>35</sup> and indeed corresponds to the previously determined DFT calculated value of  $a = b = 3.328 \text{ \AA}$ .<sup>23</sup> The optimized V–Se bond length is  $2.487 \text{ \AA}$  with the computed interlayer distance of  $1.84 \text{ \AA}$ , matching the earlier available interlayer result of  $1.56 \text{ \AA}$ .<sup>35</sup> The TDOS of  $\text{VSe}_2$  have been calculated using the GGA + U approach (U value  $\approx 3.5$  eV for V<sup>36</sup>) and are displayed in Fig. 2. The continuous and asymmetric spin states at

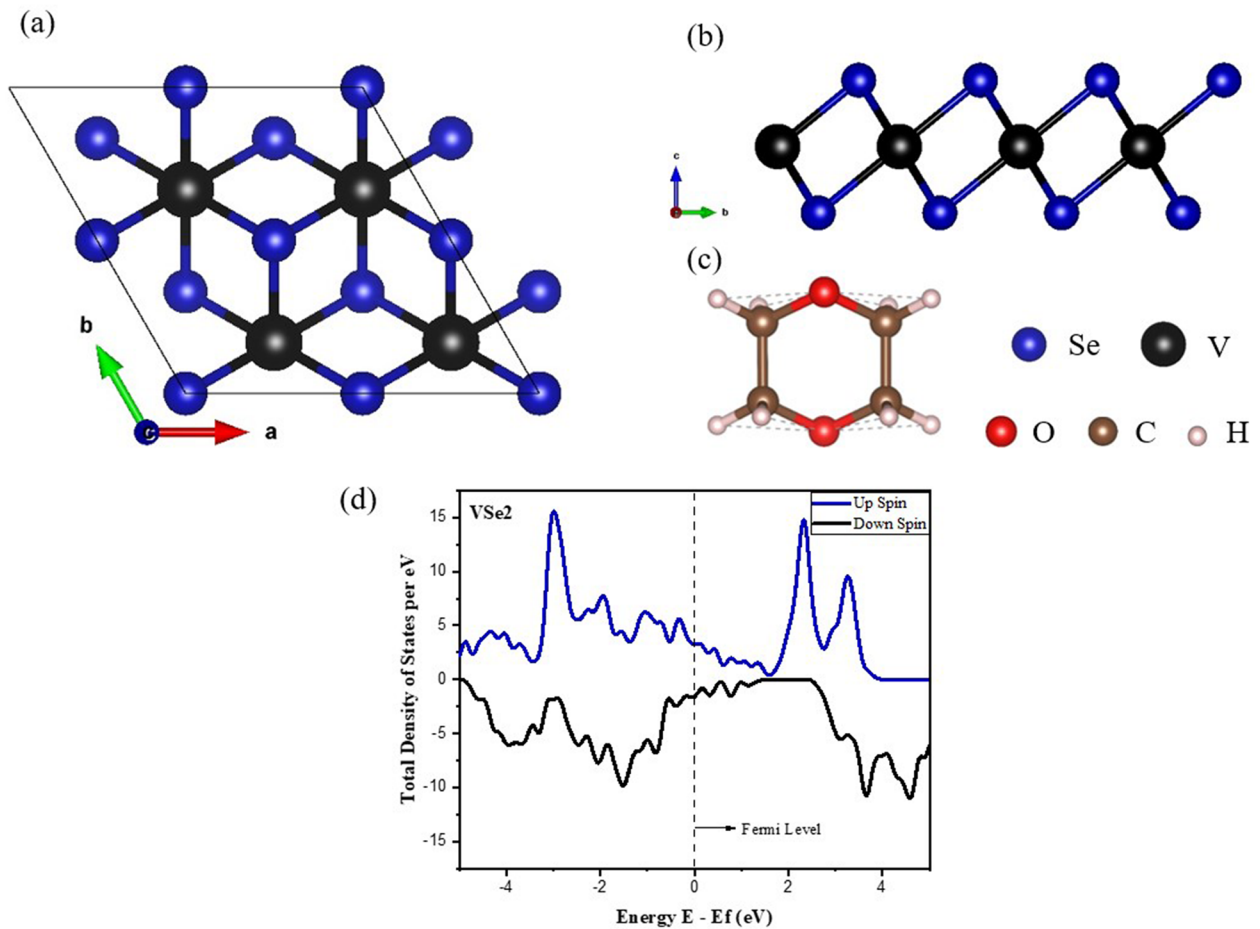


**FIG. 1.** The geometrically optimized structure of 1T  $\text{VSe}_2$  monolayer in (a) armchair and (b) zigzag, (c) the relaxed structure of dioxane molecule, and (d) TDOS plot of 1T  $\text{VSe}_2$ .

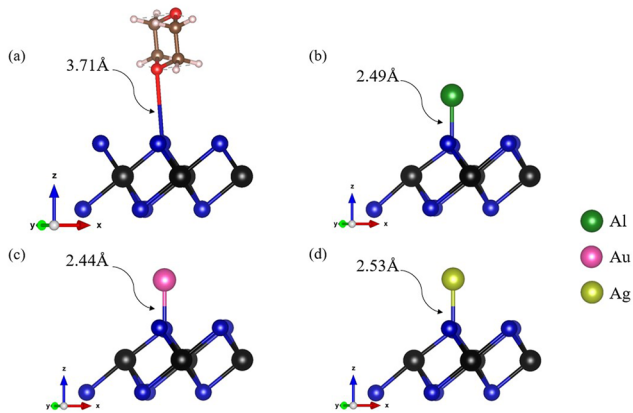


**FIG. 2.** Optimized structures of (a) dioxane adsorbed pristine  $\text{VSe}_2$  and metal-doped  $\text{VSe}_2$  after geometrical relaxation, (b) Al, (c) Au, and (d) Ag.

the Fermi level indicate that 1T  $\text{VSe}_2$  is magnetic and metallic.<sup>35</sup> The reasonable match of pristine  $\text{VSe}_2$  bond length and other electronic parameters with previously reported results gives us confidence in the simulation procedures and methods' accuracy. 1T  $\text{MX}_2$  structure shows two major directions, armchair and zigzag. For the monolayer 1T  $\text{VSe}_2$ , the zigzag direction shows significantly stronger and more stretchy than armchair<sup>37</sup> [see Fig. 1(b)].

### B. Adsorption studies of dioxane on pristine $\text{VSe}_2$

Here, we have placed the dioxane molecule  $\sim 2 \text{ \AA}$  above the surface of the pristine  $\text{VSe}_2$  at four different adsorption sites: hcp, fcc, top, and hollow sites.<sup>37</sup> Several combinations of the initial structures were explored; for example, the O atom of the dioxane molecule is close to the different sites of  $\text{VSe}_2$  and is geometrically relaxed to minimum energy configuration. The most stable geometric

**TABLE I.** DFT calculated adsorption energy and bond length of metal-doped  $\text{VSe}_2$  systems.

System	Adsorption energy (eV)	Bond length ( $\text{\AA}$ )
$\text{VSe}_2 + \text{Ti}$	+3.623	2.340 (Se-Ti)
$\text{VSe}_2 + \text{W}$	+7.388	2.285 (Se-W)
$\text{VSe}_2 + \text{Al}$	-2.158	2.495 (Se-Al)
$\text{VSe}_2 + \text{Au}$	-1.412	2.437 (Se-Au)
$\text{VSe}_2 + \text{Ag}$	-1.124	2.534 (Se-Ag)

structure of  $\text{VSe}_2 + \text{dioxane/dopant}$  is attained by the adsorption energy ( $E_{ad}$ ) calculation using the following expression:

$$E_{ad}(D) = E(\text{VSe}_2 + D) - E(\text{VSe}_2) - E(D), \quad (1)$$

where  $E(\text{VSe}_2)$ ,  $E(D)$ , and  $E(\text{VSe}_2 + D)$  are, respectively, the energies of pristine  $\text{VSe}_2$ , dioxane molecule or dopant, and  $\text{VSe}_2 + \text{dioxane/dopant}$  system. Figure 2(a) depicts the DFT optimized structure of dioxane adsorbed  $\text{VSe}_2$ . The top site of Se with adsorption energy of  $-0.15 \text{ eV}$  at a bond distance of  $3.71 \text{ \AA}$  is found to be the most favorable position for the dioxane adsorption. The adsorption energy is negative, indicating that the adsorption is spontaneous and energetically feasible. The Density of States (DOS) of the  $\text{VSe}_2$  gets altered after the dioxane adsorption, and it is clearly visible in Fig. 3(b). The adsorption configuration of dioxane molecules on the  $\text{VSe}_2$  monolayer results in the transfer of charges between them. The LCA is performed to quantify the charge transfer between the dioxane and the pristine  $\text{VSe}_2$  monolayer. As per the LCA, only a minute charge of  $0.041e$  transfers from the  $\text{VSe}_2$  to the dioxane molecule. The negligible charge transfer, weak adsorption energy, and large interaction distance suggest that the dioxane adsorption on pristine  $\text{VSe}_2$  monolayer is physisorption, which would be due to the long-range van der Waal's forces. The practical implementation of the sensor requires

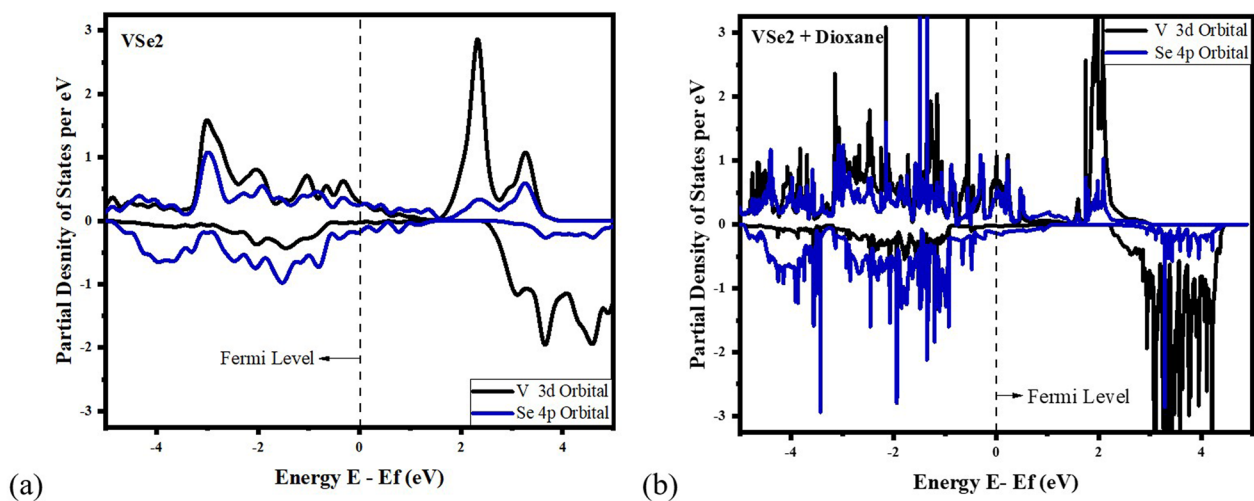


**FIG. 3.** PDOS plots of (a) pristine and (b) dioxane adsorbed  $\text{VSe}_2$ .

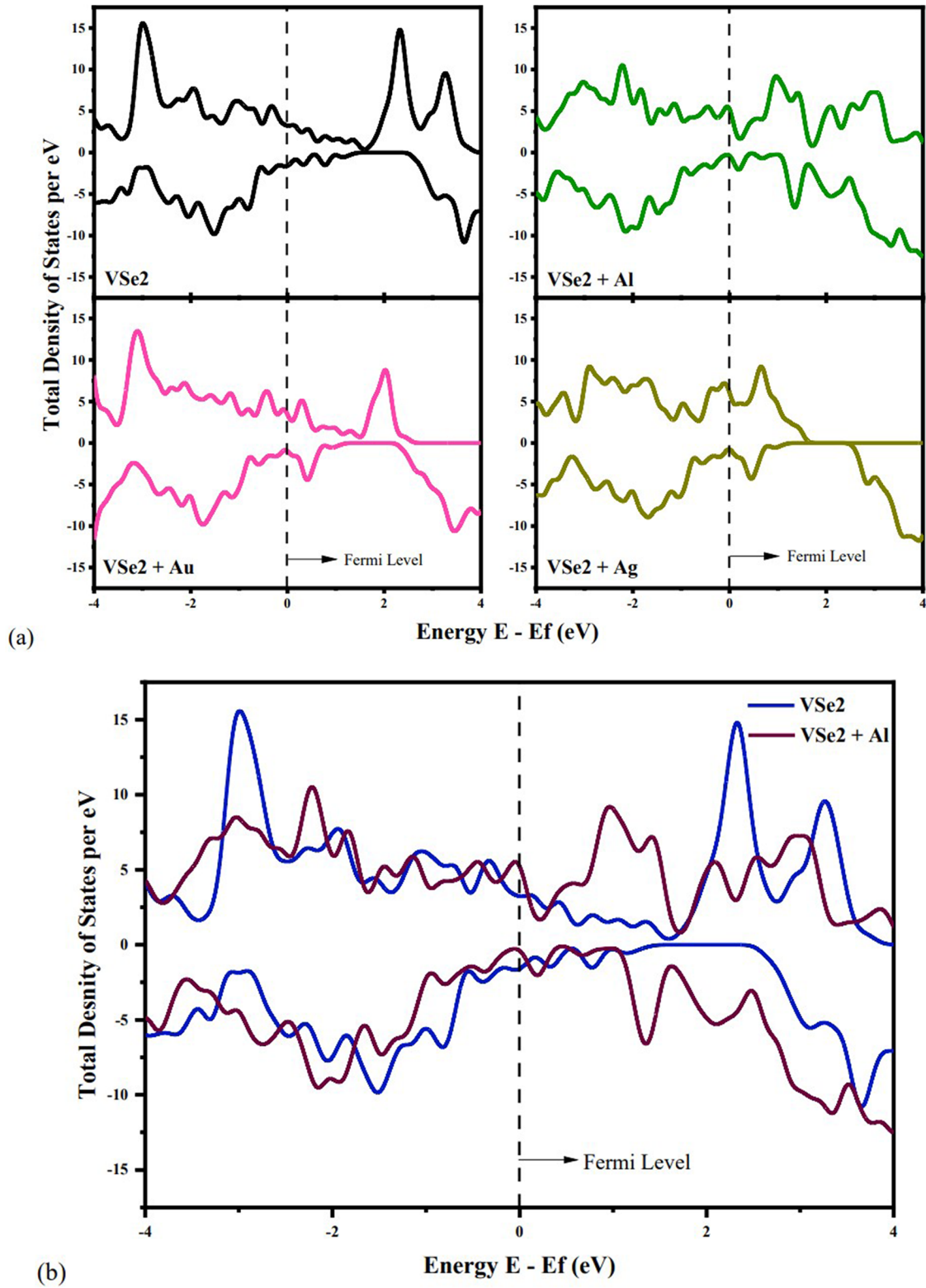


FIG. 4. TDOS plots for (a) pristine VSe<sub>2</sub>, VSe<sub>2</sub> + Al, VSe<sub>2</sub> + Au, and VSe<sub>2</sub> + Ag systems (b) merged plots of pristine VSe<sub>2</sub> and VSe<sub>2</sub> + Al.

the dioxane molecules to be adsorbed strongly on the surface. In this respect, a metallic doping strategy was adopted.

### C. Modification of the VSe<sub>2</sub> monolayer by metallic doping

We have placed metals, such as Al, Ag, Au, W, and Ti  $\sim 2$  Å, above the VSe<sub>2</sub> surface at different adsorption sites and allowed the systems to relax. The adsorption energies and bond lengths for the best configuration of VSe<sub>2</sub> + metal are calculated using Eq. (1) and are shown in Table I. From adsorption calculations at different sites, it was found that the top site above the Se atom was the best site for doped metals Al, Au, and Ag. The W and Ti showed positive adsorption energies, implying that they do not bind on the VSe<sub>2</sub> surface. The corresponding relaxed structures of the metal-doped VSe<sub>2</sub> monolayer are illustrated in Figs. 2(b)–2(d). As per the calculated adsorption energy values, Al binds strongly on the VSe<sub>2</sub> monolayer with an energy of  $-2.158$  eV. At the same time, the Au and Ag have comparatively low adsorption energy of  $-1.412$

and  $-1.124$  eV, respectively. Hence, the adsorption energy analysis confirms Al as the best dopant. Figure 4(a) denotes the TDOS of pristine and metal-doped VSe<sub>2</sub> systems. The improvement of energy states close to the Fermi level indicates the increase in conductivity of metal-doped VSe<sub>2</sub>. The asymmetric spin states in the TDOS of VSe<sub>2</sub> + metal reminds the persistence of the magnetic nature. Additionally, Fig. 4(b) plots the TDOS plots of the pristine VSe<sub>2</sub> merged with the Al-doped VSe<sub>2</sub>. Unlike the original VSe<sub>2</sub> monolayer, the DOS of the Al-doped system differs in several energy levels, with some significant increase in the Fermi level, which may be due to the electron exchange between the VSe<sub>2</sub> monolayer to the Al atom.

The PDOS analysis provides a clear idea of the orbital interactions and the direction of transfer of charges between the dioxane molecule and the substrate VSe<sub>2</sub>. Figure 5 compares PDOS of the valance orbitals of VSe<sub>2</sub> (V 3d orbital and Se 4p orbital), 3p orbitals of isolated Al atom and Al atom in the VSe<sub>2</sub> + Al system. When the Al atom binds to the VSe<sub>2</sub> surface, a reduction in the energy states of the Al 3p orbital at the Fermi level occurs compared to that in the isolated Al atom. Simultaneously, the V 3d and Se 4p near the Fermi

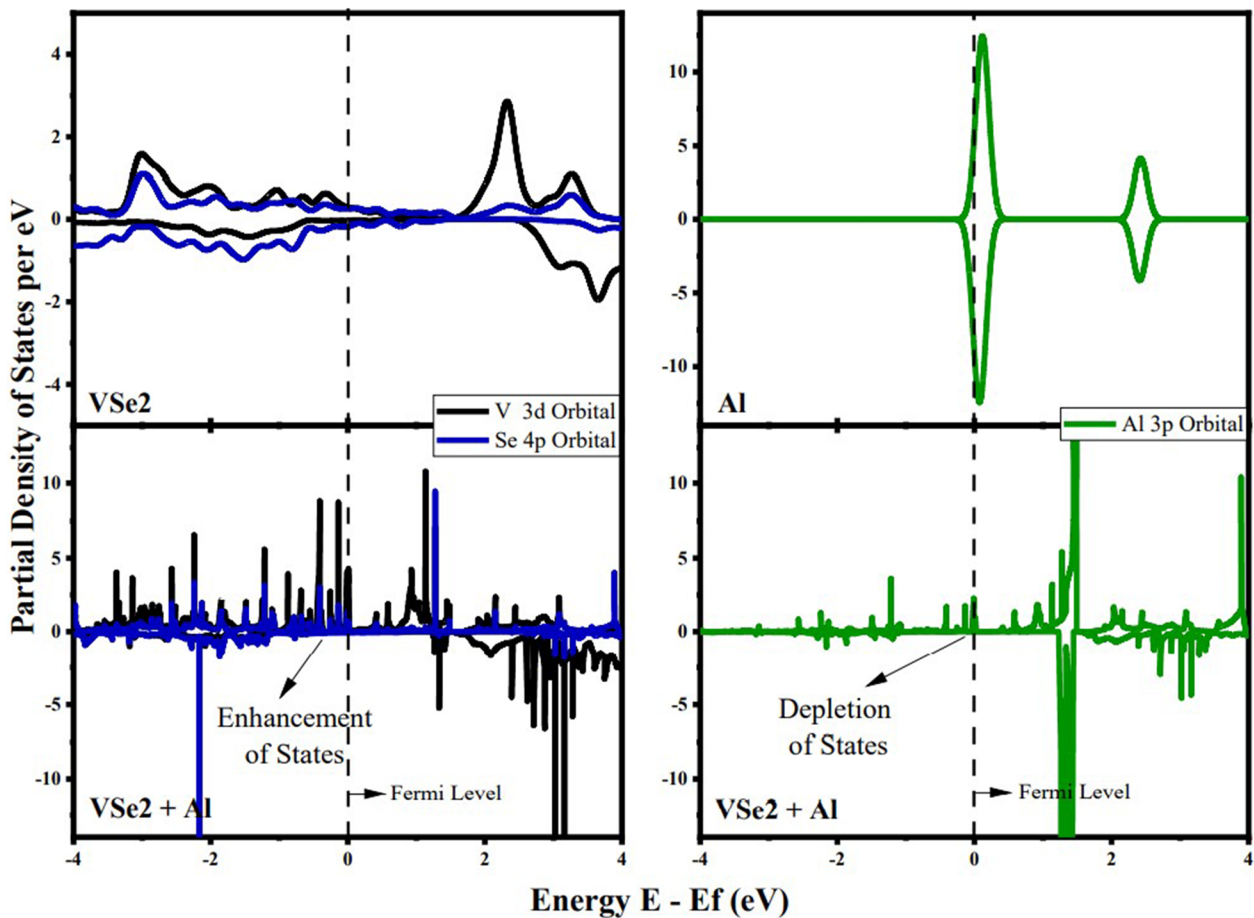


FIG. 5. The PDOS plots compare the valence orbitals of VSe<sub>2</sub> in the pristine and Al + VSe<sub>2</sub> system in the left panel, whereas in the right panel compare the 3p orbitals of isolated Al atom and the Al + VSe<sub>2</sub> system.



level get magnified, and the overall states are redistributed. This reduction in the Al and enhancement in  $VSe_2$  energy states signifies a charge transfer from Al  $3p$  orbital to  $4p$  and  $3d$  orbitals of Se and V in  $VSe_2$  and is a result of the existence of an unpaired valence electron in the outermost  $p$  orbital. Hence, the Al atom tends to donate the electron and become an anion.

A similar redistribution of states can be observed from the PDOS plots of Au- and Ag-doped  $VSe_2$  systems (supplementary material, Fig. S1). Since Au and Ag have an unpaired electron in

their valence  $s$  orbitals, they can either act as an electron donor or an acceptor. On interacting with the  $VSe_2$  system, the energy states of both the metals got depleted around the Fermi level (right panel of Fig. S1). This indicates the charge donating behavior of the Au and Ag metals. At the same time, the increased energy states near the Fermi level of the valence orbitals of the V and Se in  $VSe_2$  denote the charge accumulation (left panel of Fig. S1), i.e., the  $VSe_2$  gains charge from Au and Ag's  $6s$  and  $5s$  orbitals, respectively. According to the LCA, the Al atom loses a charge of  $0.299e$  to the  $VSe_2$  system.

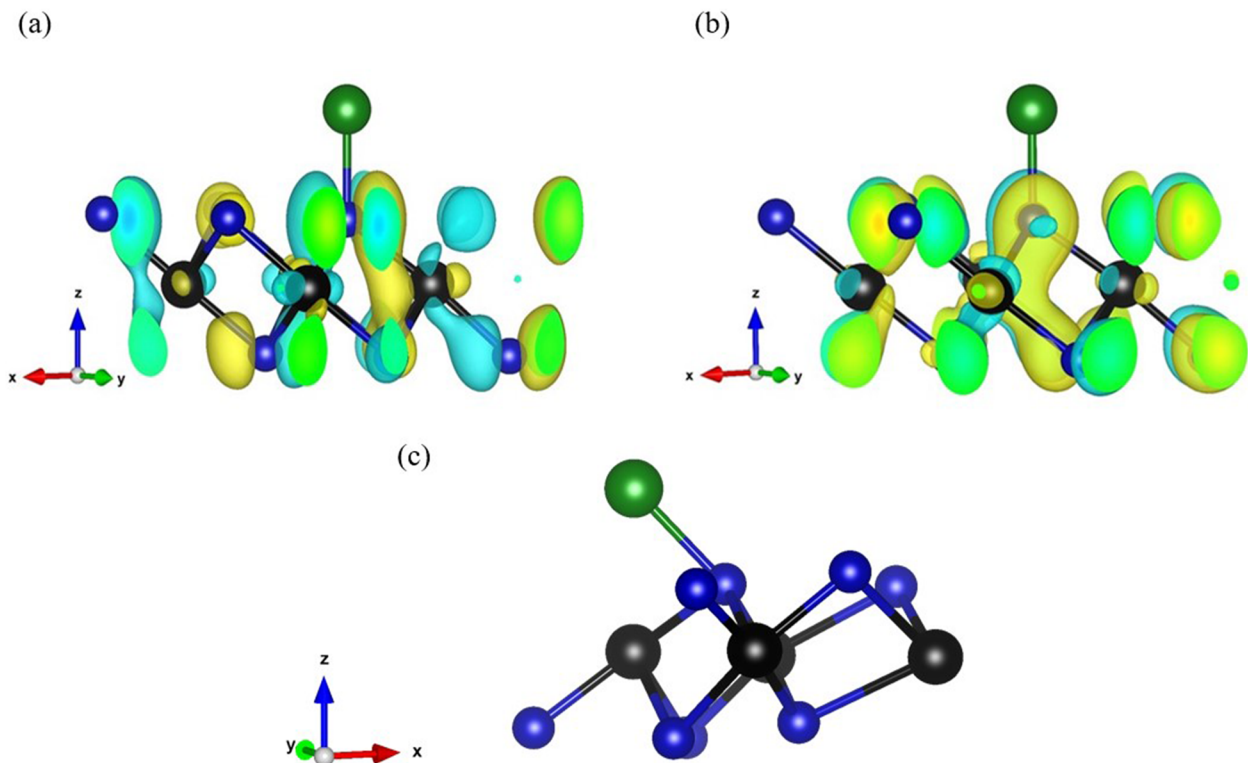


FIG. 6. The HOMO (a), LUMO (b), figures and MD snapshot at 300 K (c) of Al-doped  $VSe_2$ .

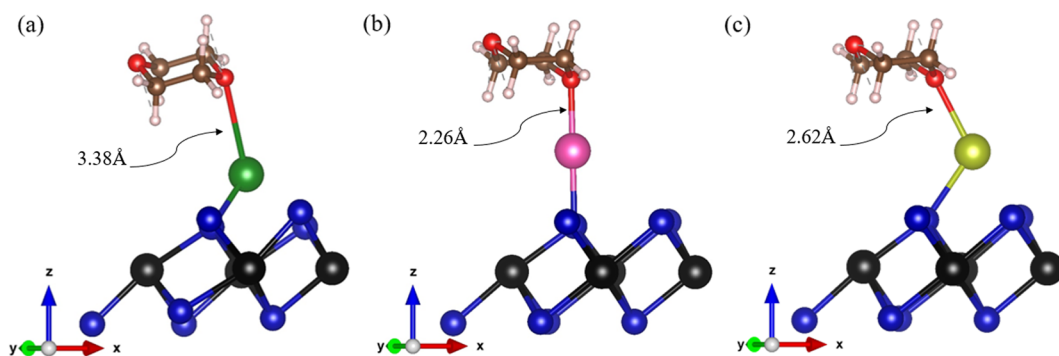


FIG. 7. Optimized structures of dioxane adsorbed (a)  $VSe_2 + Al$ , (b)  $VSe_2 + Au$ , and (c)  $VSe_2 + Ag$  systems.

In contrast, Au and Ag lose about  $0.173e$  and  $0.145e$ , respectively, to  $VSe_2$  systems. The results obtained from LCA are pretty consistent with the PDOS.

Figures 6(a) and 6(b), respectively, shows the HOMO (highest occupied molecular orbital) and LUMO (lowest unoccupied molecular orbital) distributions of the Al-doped  $VSe_2$  system. It is noted that a significant portion of HOMO and LUMO, basically the electron receiving/donating part, is distributed near the Se atom to which the Al is bonded. This signifies that the addition of Al atom enriched the active region on the  $VSe_2$  surface and hence the sensitivity of the material. All the DFT calculations were performed at 0 K; therefore, it is highly essential to see the structural stability at ambient temperatures. Desorption of the molecules from the sensor materials is usually achieved by heating the material to higher temperatures. This also requires the consistency of the system at a higher temperature. To establish the same, we performed the *ab initio* Molecular Dynamics (AIMD) simulations at 300 K for the best system, i.e.,  $VSe_2 + Al$  system. Figure 6(c) depicts the MD snapshot of the  $VSe_2 + Al$  system for 3 ps. Although the structural plot of  $VSe_2 + Al$  shows minor bond length variations due to the

**TABLE II.** The adsorption energy and bond length of dioxane adsorbed pristine and metal-doped  $VSe_2$  systems.

System	Adsorption energy (eV)	Bond length (Å)
Pristine $VSe_2 +$ dioxane	-0.15	3.71 (Se-O)
$VSe_2 + Al +$ dioxane	-0.80	3.38 (Al-O)
$VSe_2 + Au +$ dioxane	-0.30	2.26 (Au-O)
$VSe_2 + Ag +$ dioxane	-0.20	2.62 (Ag-O)

thermal agitations, the system remains stable without any distortion at 300 K. Therefore, the Al-doped  $VSe_2$  system is quite feasible for practical sensor applications.

#### D. Adsorption of dioxane on metal-doped $VSe_2$

To observe the dioxane adsorption on the metal-doped  $VSe_2$  system, we have placed the dioxane molecule above the structurally

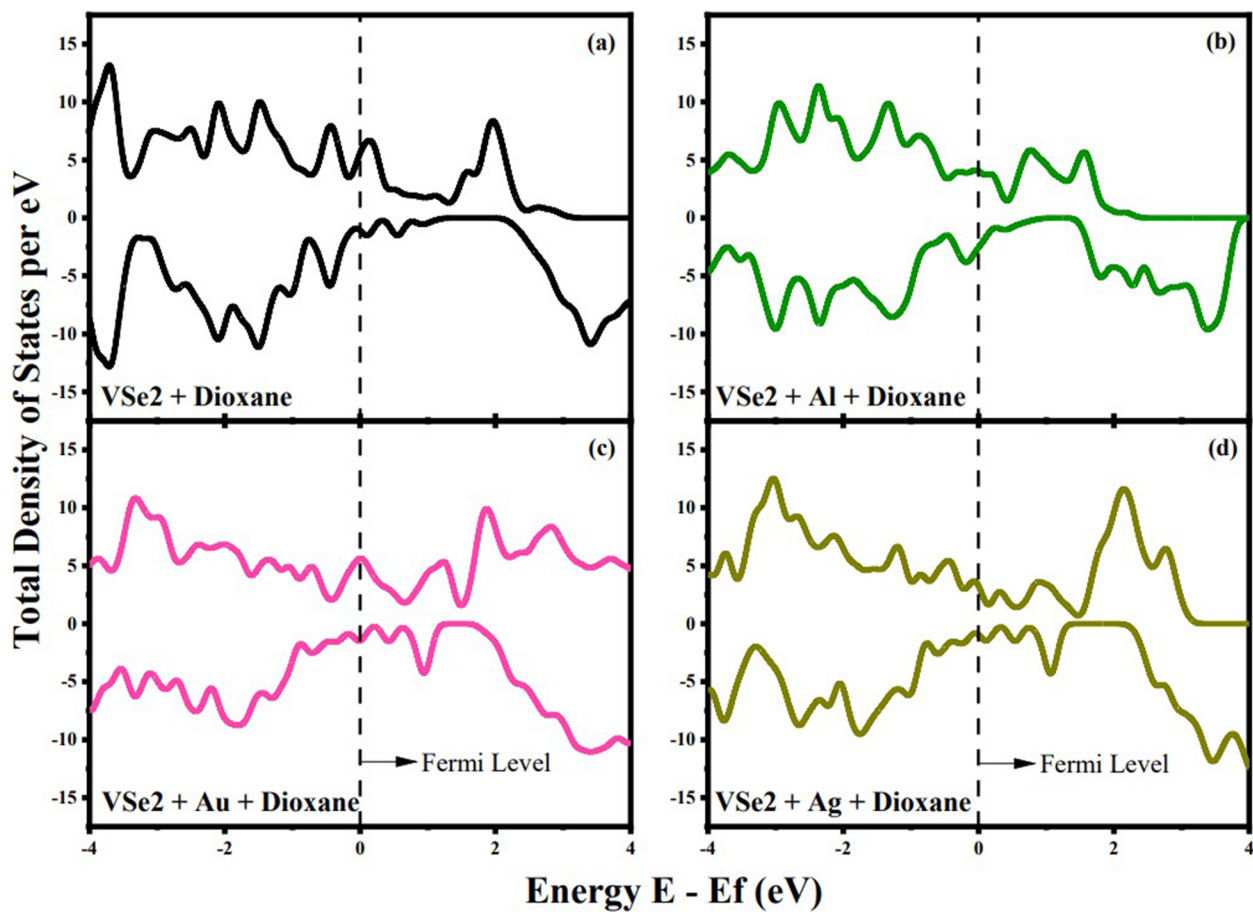


**FIG. 8.** TDOS plots of dioxane interaction on (a) pristine  $VSe_2$ , (b)  $VSe_2 + Al$ , (c)  $VSe_2 + Au$ , and (d)  $VSe_2 + Ag$  systems.

relaxed metal-doped  $\text{VSe}_2$  system such that the distance between the metal and the molecule is  $\sim 2$  Å. The resulting structural combinations are allowed to optimize geometrically. The corresponding structures in their minimum energy configurations are shown in Fig. 7.

The adsorption energy and bond length of dioxane on different  $\text{VSe}_2$  systems are tabulated (Table II). The dioxane has a greater binding on the Al-doped system with an adsorption energy of  $-0.8$  eV. This high energy value indicates that dioxane molecules chemisorb on the Al-doped system. While dioxane adsorption on the Ag- and Au-doped  $\text{VSe}_2$  systems are mostly physisorption, the adsorption energies are  $-0.30$  and  $-0.20$  eV, respectively. It is also noted that the dioxane adsorption strength increases by the strategy of metal doping, which in turn signifies the improvement in the sensing activity of the pristine  $\text{VSe}_2$  system. The shortest distance between the O atom of the dioxane molecule and the Al atom in the  $\text{VSe}_2 + \text{Al}$  system is  $3.38$  Å. While the O–Au and O–Ag distances are  $2.26$  and  $2.62$  Å, respectively. The adsorption energy calculations conclude that the Al-doped  $\text{VSe}_2$  system is well suited as the sensor material for detecting dioxane molecules from the atmosphere.

### E. Mechanism of dioxane adsorption in metal-doped $\text{VSe}_2$ system

The DOS analysis explains how the electronic structure of the metal-doped  $\text{VSe}_2$  system varies with the dioxane adsorption. Figure 8 compares the TDOS of the pristine and metal-doped  $\text{VSe}_2$  system after the dioxane adsorption. The main reason for the origin of new energy states of the pristine and metal-doped  $\text{VSe}_2$  system near the Fermi level is mainly because of the presence of dioxane molecules on its surface.

We have also analyzed the PDOS to clarify the orbital level interactions and charge transfer in the metal-doped  $\text{VSe}_2$  systems. The PDOS of the Al  $3p$  orbitals of  $\text{VSe}_2 + \text{Al}$  and  $\text{VSe}_2 + \text{Al} + \text{dioxane}$  systems are shown in the left top and bottom panel, respectively, in Fig. 9. At the same time, the right upper panel of the same figure represents the PDOS for the O  $2p$  orbitals of the isolated dioxane, and the lower panel compares the PDOS for the O  $2p$  orbitals of the  $\text{VSe}_2 + \text{Al} + \text{dioxane}$  system. It is worth noting that, after the interaction of the dioxane molecule with the  $\text{VSe}_2 + \text{Al}$  system, the energy states around the Fermi level of the Al  $3p$  orbital diminished. At the same time, new states originated around the Fermi level of

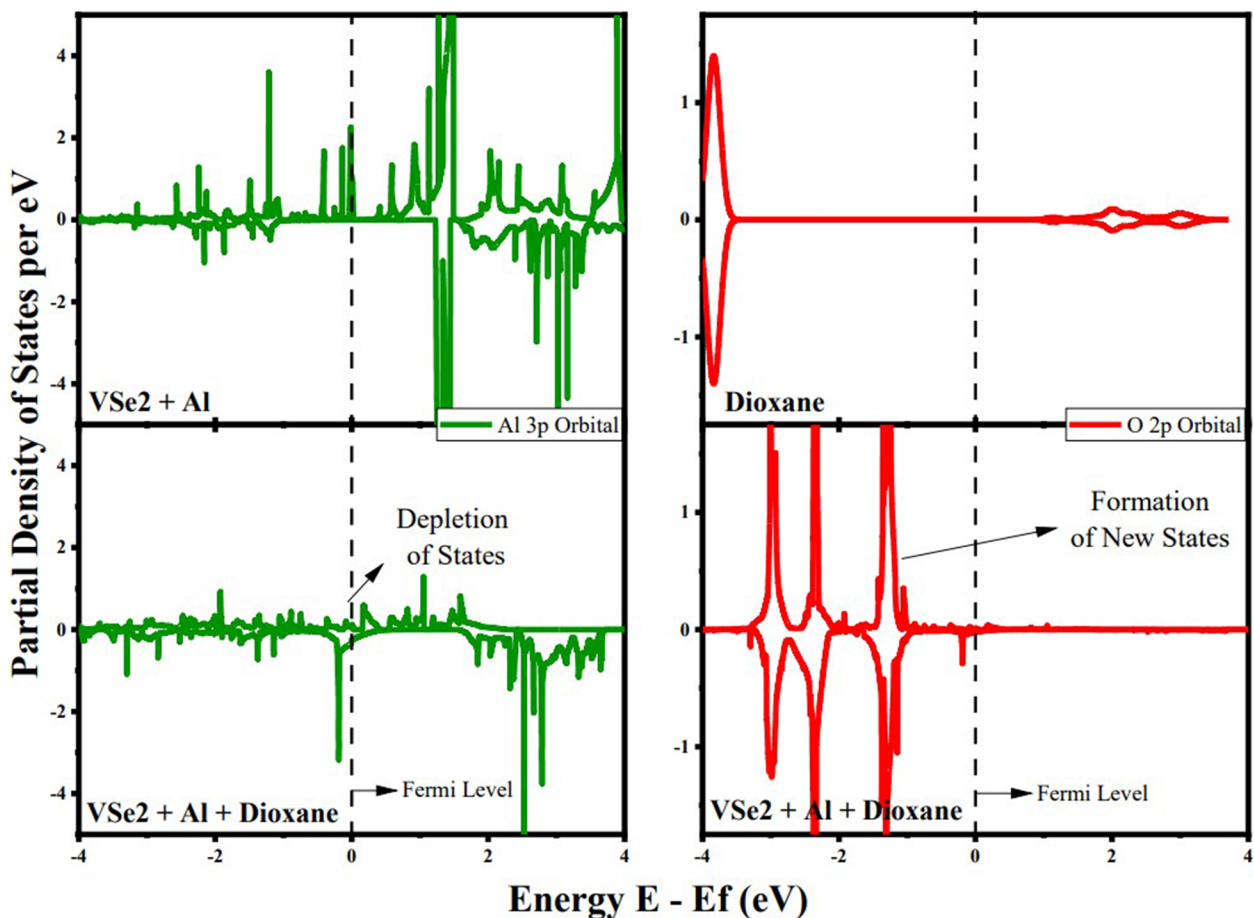


**FIG. 9.** Orbital interaction analysis of  $\text{VSe}_2 + \text{Al} + \text{dioxane}$  using PDOS plots, compare the valence orbitals of Al in the  $\text{VSe}_2 + \text{Al}$  and  $\text{VSe}_2 + \text{Al} + \text{dioxane}$  system in the left panel. In contrast, the right panel compares the  $2p$  orbitals of isolated dioxane atoms and the  $\text{VSe}_2 + \text{Al} + \text{dioxane}$  systems.



**TABLE III.** LCA information on charge transfer of  $VSe_2$  + metal systems to the dioxane molecule.

System	Charge transfer
$VSe_2$ + Al + dioxane	$-0.567e$ (Al 3 <i>p</i> orbital – O 2 <i>p</i> orbital)
$VSe_2$ + Au + dioxane	$-0.101e$ (Au 6 <i>s</i> orbital – O 2 <i>p</i> orbital)
$VSe_2$ + Ag + dioxane	$-0.132e$ (Ag 5 <i>s</i> orbital – O 2 <i>p</i> orbital)

the O 2*p* orbital. These states were absent in the same energy range of the PDOS of isolated dioxane. This formation of new states in the O 2*p* orbital and decrement in the intensity of available energy states in the Al 3*p* orbital implies that the electronic charges are transferred from the O 2*p* to Al 3*p* orbital. In addition, the strong dioxane adsorption is because of the p-p orbital overlap. The quantitative charge transfer study by LCA also justifies this charge transfer, i.e.,  $\sim 0.567e$  charges are lost by the 3*p* orbitals of Al in the  $VSe_2$  + Al system to the O 2*p* orbital of the dioxane molecule.

A comparable reallocation of the energy states is observed in the PDOS of  $VSe_2$  + Au and  $VSe_2$  + Ag systems after the dioxane adsorption (Fig. S2). Similar to the Al 3*p* orbitals, the energy states of Ag 5*s* and Au 6*s* orbitals near the Fermi level decrease. Meanwhile, there is an enhancement in the energy states in the vicinity of the Fermi level of O 2*p* orbital of dioxane in the adsorbed system. The charge transfer from Ag and Au's *s* orbitals to the O 2*p* orbitals causes this reduction and enhancement in states. According to LCA, Au 6*s* lose 0.101*e*, and Ag 5*s* lose 0.132*e* charges to the O 2*p* orbital of dioxane, shown in Table III.

A large amount of charge transfer between the Al-doped  $VSe_2$  system and dioxane molecule is due to the strong chemical adsorption. The minor charge transfer from the Ag and Au to the dioxane molecule is due to the physisorption. Since adsorption energy and charge transfer are the important parameters in sensing, the Al-doped  $VSe_2$  system will be beneficial for the fabrication of electrochemical dioxane sensors.

#### IV. CONCLUSION

In conclusion, we used the first principle density functional theory technique to explore the dioxane sensing abilities of pristine and metal-doped (Al, Au, and Ag) 2D  $VSe_2$  systems. We have investigated various adsorption sites of the dioxane molecules on the pristine  $VSe_2$  surface. Our adsorption energy calculation suggests that the dioxane interaction is more with the metal-doped  $VSe_2$  system, particularly the Al-doped  $VSe_2$ , than its pristine counterpart. The Al atom binds strongly on the  $VSe_2$  surface than the other metals with higher energy and charge transfer. The metal doping improved the conductivity and hence the adsorption ability of the  $VSe_2$  system. The strong adsorption of the dioxane molecules with the  $VSe_2$  + Al system is mainly due to the extensive charge transport and orbital interaction between the O 2*p* of dioxane and the 3*p* orbitals of Al. The MD simulation at 300 K verified the room temperature stability of the  $VSe_2$  + Al system; therefore, the Al-doped  $VSe_2$  system could be a more promising dioxane sensor. This work aims to provide a theoretical foundation and an interpretation of the adsorption behaviors of  $VSe_2$ -based biosensors to facilitate future empirical creations.

#### SUPPLEMENTARY MATERIALS

See the [supplementary material](#) for the PDOS analysis of Au and Ag doping in pristine  $VSe_2$  and the dioxane interaction on Au and Ag doped  $VSe_2$ .

#### ACKNOWLEDGMENTS

N.K. acknowledges SERB: CRG (Grant No. CRG/2021/001506), UGC: Special Assistance Program (SAP; Grant Nos. F.530/12/DRS/2009 and F.530/13/DRS II/2016), UGC: Scheme for Promotion of Academic and Research Collaboration (SPARC; Grant Nos. P930, P1400, P1429, and P1460), DST: Nano Mission [Grant No. SR/NM/NS-1420-2014(C)], DST: Fund for Improvement of S&T Infrastructure (FIST; Grant No. SR/FST/P SI-143/2009), DAE: UGC-Consortium for Scientific Research (CSR; Grant No. UGC-DAE-CSR-KC/CRS/19/RC08/0983/1018), DAE-Board of Research in Nuclear Sciences (BRNS; Grant No. 39/29/2015-BRNS/39009), and DST Promotion of University Research and Scientific Excellence [PURSE; Grant No. SR/S9/Z-23/2010/22(C, G)], Government of India programs for providing the facilities for research and development in IIUCNN, MGU. The authors would like to thank the High-Performance Computing facilities provided by MGU.

#### AUTHOR DECLARATIONS

##### Conflict of Interest

The authors have no conflicts to disclose.

#### Author Contributions

**Sreejith Pallikkara Chandrasekharan:** Conceptualization (equal); Data curation (equal); Formal analysis (equal); Funding acquisition (equal); Investigation (equal); Methodology (equal); Software (equal); Visualization (equal); Writing – original draft (equal); Writing – review & editing (equal). **Seetha Lakshmy:** Conceptualization (equal); Data curation (equal); Formal analysis (equal); Investigation (equal); Methodology (equal); Software (equal); Writing – original draft (equal); Writing – review & editing (equal). **Saju Joseph:** Conceptualization (equal); Data curation (equal); Formal analysis (equal); Investigation (equal); Methodology (equal); Project administration (equal); Software (equal); Supervision (equal); Writing – original draft (equal); Writing – review & editing (equal). **Nandakumar Kalarikkal:** Conceptualization (equal); Formal analysis (equal); Funding acquisition (equal); Project administration (equal); Resources (equal); Supervision (equal); Validation (equal); Writing – original draft (equal).

#### DATA AVAILABILITY

The data that support the findings of this study are available from the corresponding authors upon reasonable request.

## REFERENCES

- <sup>1</sup>A. Fullana, J. A. Conesa, R. Font, and S. Sidhu, "Formation and destruction of chlorinated pollutants during sewage sludge incineration," *Environ. Sci. Technol.* **38**(10), 2953–2958 (2004).
- <sup>2</sup>H.-S. Inaki, "Exploring the dissemination of environmental certifications in high and low polluting industries," *J. Cleaner Prod.* **89**, 50–58 (2015).
- <sup>3</sup>R. Hu, S. Dai, D. Shao, A. Alsaedi, B. Ahmad, and X. Wang, "Efficient removal of phenol and aniline from aqueous solutions using graphene oxide/polypyrrole composites," *J. Mol. Liq.* **203**, 80–89 (2015).
- <sup>4</sup>K. J. Godri Pollitt, J.-H. Kim, J. Peccia, M. Elimelech, Y. Zhang, G. Charkoftaki, B. Hodges, I. Zucker, H. Huang, N. C. Deziel, K. Murphy, M. Ishii, C. H. Johnson, A. Boissevain, E. O'Keefe, P. T. Anastas, D. Orlicky, D. C. Thompson, and V. Vasilou, "1,4-dioxane as an emerging water contaminant: State of the science and evaluation of research needs," *Sci. Total Environ.* **690**, 853–866 (2019).
- <sup>5</sup>D. K. Stepien, P. Diehl, J. Helm, A. Thoms, and W. Püttmann, "Fate of 1,4-dioxane in the aquatic environment: From sewage to drinking water," *Water Res.* **48**, 406–419 (2014).
- <sup>6</sup>S. Zhang, P. B. Gedalanga, and S. Mahendra, "Advances in bioremediation of 1,4-dioxane-contaminated waters," *J. Environ. Manage.* **204**, 765–774 (2017).
- <sup>7</sup>M. A. Beckett and I. Hua, "Elucidation of the 1,4-dioxane decomposition pathway at discrete ultrasonic frequencies," *Environ. Sci. Technol.* **34**(18), 3944–3953 (2000).
- <sup>8</sup>U. Karges, D. Ott, S. De Boer, and W. Püttmann, "1,4-dioxane contamination of German drinking water obtained by managed aquifer recharge systems: Distribution and main influencing factors," *Sci. Total Environ.* **711**, 134783 (2020).
- <sup>9</sup>Y. Xiong, Q. Zhang, R. Wandell, S. Bresch, H. Wang, B. R. Locke, and Y. Tang, "Synergistic 1,4-dioxane removal by non-thermal plasma followed by biodegradation," *Chem. Eng. J.* **361**, 519–527 (2019).
- <sup>10</sup>C.-S. Lee, A. K. Venkatesan, H. W. Walker, and C. J. Gobler, "Impact of groundwater quality and associated byproduct formation during UV/hydrogen peroxide treatment of 1,4-dioxane," *Water Res.* **173**, 115534 (2020).
- <sup>11</sup>M. J. Zenker, R. C. Borden, and M. A. Barlaz, "Occurrence and treatment of 1,4-dioxane in aqueous environments," *Environ. Eng. Sci.* **20**(5), 423–432 (2003).
- <sup>12</sup>M. M. Rahman, A. Wahid, and A. M. Asiri, "Development of highly sensitive 1,4-dioxane sensor with semiconductor NiO-doped  $\text{Nd}_2\text{O}_3$  nanostructures by electrochemical approach," *New J. Chem.* **43**(44), 17395–17402 (2019).
- <sup>13</sup>T. K. Sana Fathima, A. Arshiya Banu, T. Devasena, and S. Ramaprabhu, "A novel, highly sensitive electrochemical 1,4-dioxane sensor based on reduced graphene oxide–curcumin nanocomposite," *RSC Adv.* **12**(30), 19375–19383 (2022).
- <sup>14</sup>R. G. Parr, "Density functional theory of atoms and molecules," in *Horizons of Quantum Chemistry* (Springer, 1980), pp. 5–15.
- <sup>15</sup>Z. Chen, Y. Liu, S. Liao, N. Yi, and Q. Hu, "Treatment of adsorption of dioxane by using SiCNT toward efficient remediation of refractory organic contaminants from wastewater: DFT and DFTB-MD simulations," *J. Mol. Liq.* **316**, 113869 (2020).
- <sup>16</sup>Q. H. Wang, K. Kalantar-Zadeh, A. Kis, J. N. Coleman, and M. S. Strano, "Electronics and optoelectronics of two-dimensional transition metal dichalcogenides," *Nat. Nanotechnol.* **7**(11), 699–712 (2012).
- <sup>17</sup>B. Radisavljevic, A. Radenovic, J. Brivio, V. Giacometti, and A. Kis, "Single-layer  $\text{MoS}_2$  transistors," *Nat. Nanotechnol.* **6**(3), 147–150 (2011).
- <sup>18</sup>A. Vaidyanathan, S. Lakshmy, G. Sanyal, S. Joseph, N. Kalarikkal, and B. Chakraborty, "Nitrobenzene sensing in pristine and metal doped 2D dichalcogenide  $\text{MoS}_2$ : Insights from density functional theory investigations," *Appl. Surf. Sci.* **550**, 149395 (2021).
- <sup>19</sup>S. Xu, Y. Zhang, F. Xu, C. Chen, and Z. Shen, "Theoretical study of the adsorption behaviors of gas molecules on the Au-functionalized  $\text{MoS}_2$  nanosheets: A search for highly efficient gas sensors," *Comput. Theor. Chem.* **1188**, 112935 (2020).
- <sup>20</sup>S. Lakshmy, G. Sanyal, A. Vaidyanathan, S. Joseph, N. Kalarikkal, and B. Chakraborty, "Catechol detection in pure and transition metal decorated 2D  $\text{MoS}_2$ : Acumens from density functional theory approaches," *Appl. Surf. Sci.* **562**, 150216 (2021).
- <sup>21</sup>M. Chhowalla, D. Voiry, J. Yang, H. S. Shin, and K. P. Loh, "Phase-engineered transition-metal dichalcogenides for energy and electronics," *MRS Bull.* **40**(7), 585–591 (2015).
- <sup>22</sup>M. Calandra, "Chemically exfoliated single-layer  $\text{MoS}_2$ : Stability, lattice dynamics, and catalytic adsorption from first principles," *Phys. Rev. B* **88**(24), 245428 (2013).
- <sup>23</sup>M. Salavati and T. Rabczuk, "Application of highly stretchable and conductive two-dimensional 1T  $\text{VS}_2$  and  $\text{VSe}_2$  as anode materials for Li-, Na- and Ca-ion storage," *Comput. Mater. Sci.* **160**, 360–367 (2019).
- <sup>24</sup>C. Ataca, H. Şahin, and S. Ciraci, "Stable, single-layer  $\text{MX}_2$  transition-metal oxides and dichalcogenides in a honeycomb-like structure," *J. Phys. Chem. C* **116**(16), 8983–8999 (2012).
- <sup>25</sup>Z. Zhang, J. Niu, P. Yang, Y. Gong, Q. Ji, J. Shi, Q. Fang, S. Jiang, H. Li, X. Zhou, L. Gu, X. Wu, and Y. Zhang, "Van der Waals epitaxial growth of 2D metallic vanadium diselenide single crystals and their extra-high electrical conductivity," *Adv. Mater.* **29**(37), 1702359 (2017).
- <sup>26</sup>G. Sanyal, S. Lakshmy, A. Vaidyanathan, N. Kalarikkal, and B. Chakraborty, "Detection of nitrobenzene in pristine and metal decorated 2D dichalcogenide  $\text{VSe}_2$ : Perspectives from density functional theory," *Surf. Interfaces* **29**, 101816 (2022).
- <sup>27</sup>G. V. Kamarchuk, A. V. Khotkevich, V. M. Bagatsky, V. G. Ivanov, P. Molinié, A. Leblanc, and E. Faulques, "Direct determination of Debye temperature and electron-phonon interaction in 1T  $\text{VSe}_2$ ," *Phys. Rev. B* **63**(7), 073107 (2001).
- <sup>28</sup>Z. Zhang, P. Yang, M. Hong, S. Jiang, G. Zhao, J. Shi, Q. Xie, and Y. Zhang, "Recent progress in the controlled synthesis of 2D metallic transition metal dichalcogenides," *Nanotechnology* **30**(18), 182002 (2019).
- <sup>29</sup>K. Xu, P. Chen, X. Li, C. Wu, Y. Guo, J. Zhao, X. Wu, and Y. Xie, "Ultrathin nanosheets of vanadium diselenide: A metallic two-dimensional material with ferromagnetic charge-density-wave behavior," *Angew. Chem., Int. Ed.* **52**(40), 10477–10481 (2013).
- <sup>30</sup>R. Atkins, M. Dolgos, A. Fiedler, C. Grosse, S. F. Fischer, S. P. Rudin, and D. C. Johnson, "Synthesis and systematic trends in structure and electrical properties of  $[(\text{SnSe})_{1.15}]_m(\text{VSe}_2)_1$ ,  $m = 1, 2, 3$ , and 4," *Chem. Mater.* **26**(9), 2862–2872 (2014).
- <sup>31</sup>A. L. Hector, M. Jura, W. Levason, S. D. Reid, and G. Reid, "Vanadium selenoether and selenolate complexes, potential single-source precursors for CVD of  $\text{VSe}_2$  thin films," *New J. Chem.* **33**(3), 641–645 (2009).
- <sup>32</sup>P. Giannozzi, S. Baroni, N. Bonini, M. Calandra, R. Car, C. Cavazzoni, D. Ceresoli, G. L. Chiarotti, M. Cococcioni, I. Dabo, A. Dal Corso, S. de Gironcoli, S. Fabris, G. Fratesi, R. Gebauer, U. Gerstmann, C. Gougousis, A. Kokalj, M. Lazzeri, L. Martin-Samos, N. Marzari, F. Mauri, R. Mazzarello, S. Paolini, A. Pasquarello, L. Paulatto, C. Sbraccia, S. Scandolo, G. Sclauzero, A. P. Seitsonen, A. Smogunov, P. Umari, and R. M. Wentzcovitch, "QUANTUM ESPRESSO: A modular and open-source software project for quantum simulations of materials," *J. Phys.: Condens. Matter* **21**(39), 395502 (2009).
- <sup>33</sup>J. P. Perdew, K. Burke, and M. Ernzerhof, "Generalized gradient approximation made simple," *Phys. Rev. Lett.* **77**(18), 3865–3868 (1996).
- <sup>34</sup>J. Henke, F. Flicker, J. Laverock, and J. van Wezel, "Charge order from structured coupling in  $\text{VSe}_2$ ," *SciPost Phys.* **9**(4), 056 (2020).
- <sup>35</sup>A. Huang, C.-H. Chen, C.-H. Chang, and H.-T. Jeng, "Topological phase and quantum anomalous Hall effect in ferromagnetic transition-metal dichalcogenides monolayer 1T- $\text{VSe}_2$ ," *Nanomaterials* **11**(8), 1998 (2021).
- <sup>36</sup>B. Stahl and T. Bredow, "Critical assessment of the DFT + U approach for the prediction of vanadium dioxide properties," *J. Comput. Chem.* **41**(3), 258–265 (2020).
- <sup>37</sup>Y. Wang, J. Wan, W. Tian, Z. Hou, X. Gu, and Y. Wang, "Theoretical screening of  $\text{VSe}_2$  as support for enhanced electrocatalytic performance of transition-metal single atoms," *J. Colloid Interface Sci.* **590**, 210–218 (2021).